


Article

The *Anemonia sulcata* Toxin BDS-I Protects Astrocytes Exposed to A β _{1–42} Oligomers by Restoring [Ca²⁺]_i Transients and ER Ca²⁺ Signaling

Ilaria Piccialli ^{1,†}, Valentina Tedeschi ^{1,†}, Francesca Boscia ¹, Roselia Ciccone ¹, Antonella Casamassa ¹, Valeria de Rosa ¹ , Paolo Grieco ², Agnese Secondo ^{1,*} and Anna Pannaccione ^{1,*}

¹ Division of Pharmacology, Department of Neuroscience, Reproductive and Dentistry Sciences, School of Medicine, Federico II University of Naples, 80131 Napoli, Italy; piccialli.ilaria@gmail.com (I.P.); valentina.tedeschi@unina.it (V.T.); boscia@unina.it (F.B.); cicconeroselia@gmail.com (R.C.); antonella.casamassa@unina.it (A.C.); biovalder@libero.it (V.d.R.)

² Department of Pharmacy, School of Medicine, Federico II University of Naples, 80131 Napoli, Italy; paolo.grieco@unina.it

* Correspondence: secondo@unina.it (A.S.); pannacio@unina.it (A.P.)

† Ilaria Piccialli and Valentina Tedeschi equally contributed to this article.

Abstract: Intracellular calcium concentration ([Ca²⁺]_i) transients in astrocytes represent a highly plastic signaling pathway underlying the communication between neurons and glial cells. However, how this important phenomenon may be compromised in Alzheimer's disease (AD) remains unexplored. Moreover, the involvement of several K⁺ channels, including K_v3.4 underlying the fast-inactivating currents, has been demonstrated in several AD models. Here, the effect of K_v3.4 modulation by the marine toxin blood depressing substance-I (BDS-I) extracted from *Anemonia sulcata* has been studied on [Ca²⁺]_i transients in rat primary cortical astrocytes exposed to A β _{1–42} oligomers. We showed that: (1) primary cortical astrocytes expressing K_v3.4 channels displayed [Ca²⁺]_i transients depending on the occurrence of membrane potential spikes, (2) BDS-I restored, in a dose-dependent way, [Ca²⁺]_i transients in astrocytes exposed to A β _{1–42} oligomers (5 μ M/48 h) by inhibiting hyperfunctional K_v3.4 channels, (3) BDS-I counteracted Ca²⁺ overload into the endoplasmic reticulum (ER) induced by A β _{1–42} oligomers, (4) BDS-I prevented the expression of the ER stress markers including active caspase 12 and GRP78/BiP in astrocytes treated with A β _{1–42} oligomers, and (5) BDS-I prevented A β _{1–42}-induced reactive oxygen species (ROS) production and cell suffering measured as mitochondrial activity and lactate dehydrogenase (LDH) release. Collectively, we proposed that the marine toxin BDS-I, by inhibiting the hyperfunctional K_v3.4 channels and restoring [Ca²⁺]_i oscillation frequency, prevented A β _{1–42}-induced ER stress and cell suffering in astrocytes.

Keywords: astrocytes; A β _{1–42} oligomers; BDS-I; [Ca²⁺]_i transients; ER stress; K_v3.4 channel

Key Contribution: The marine toxin BDS-I, inhibiting the hyperfunctional K_v3.4 channels and restoring [Ca²⁺]_i transients, prevented A β _{1–42}-induced ER stress in astrocytes.



Citation: Piccialli, I.; Tedeschi, V.; Boscia, F.; Ciccone, R.; Casamassa, A.; de Rosa, V.; Grieco, P.; Secondo, A.; Pannaccione, A. The *Anemonia sulcata* Toxin BDS-I Protects Astrocytes Exposed to A β _{1–42} Oligomers by Restoring [Ca²⁺]_i Transients and ER Ca²⁺ Signaling. *Toxins* **2021**, *13*, 20. <https://doi.org/10.3390/toxins13010020>

Received: 30 November 2020

Accepted: 24 December 2020

Published: 31 December 2020

Publisher's Note: MDPI stays neutral with regard to jurisdictional claims in published maps and institutional affiliations.



Copyright: © 2020 by the authors. Licensee MDPI, Basel, Switzerland. This article is an open access article distributed under the terms and conditions of the Creative Commons Attribution (CC BY) license (<https://creativecommons.org/licenses/by/4.0/>).

1. Introduction

Astrocytes, the most abundant glial cells in the central nervous system (CNS), may support neuronal homeostasis, not only releasing trophic factors, but also regulating neurotransmission and synaptic plasticity [1–7]. Moreover, astrocytes continuously handle gliotransmitters like purines, D-serine, and glutamate, whose uptake and release are regulated by the frequency of their intracellular calcium concentration ([Ca²⁺]_i) transients, a complex ionic phenomenon involving both extracellular and intracellular compartments including the endoplasmic reticulum (ER).

[Ca²⁺]_i transients in astrocytes spread throughout gap junctions belonging to the astrocytic syncytium [8–10]. Clearly, the extent of this electric phenomenon is driven by

several molecular mechanisms residing in astrocytes [11–13]. Firstly, $[Ca^{2+}]_i$ transients may be generated by the release of Ca^{2+} from ER [14] or by an influx from the extracellular space through ionotropic receptors or plasma membrane channels [12]. While the origin of ER-mediated Ca^{2+} transients seems to be predominant in the soma, the plasmalemmal-located entry mechanisms are also involved at the level of astrocyte processes [13,15–18].

Since 1965, it has been established that astrocytes can modulate neuronal activity by buffering plateau level of extracellular K^+ in the brain, thus controlling neuronal excitability [19,20]. Accordingly, defects in astrocytic K^+ buffering properties have been linked to epilepsy [21] and ischemia-dependent cell death [22]. Although well-established at neuronal level, the involvement of voltage-gated potassium (K_V) channels in the regulation of the action potential frequency and $[Ca^{2+}]_i$ transients in astrocytes is far from being fully understood, especially during the neurodegenerative process.

Moreover, defects in membrane excitability and calcium signaling represent fundamental features of many neurodegenerative disorders, including Alzheimer's disease (AD) [23]. However, how this may include the Ca^{2+} signaling machinery in astrocytes is quite obscure. In this respect, disturbance of ER Ca^{2+} homeostasis determines β -amyloid ($A\beta$) oligomer-dependent upregulation of glial fibrillary acidic protein (GFAP) expression, a widely recognized marker of astrocytic defects [24].

During neurological diseases, astrocytes undergo complex changes, which are subclassified into: (1) reactive astrogliosis, an evolutionarily conserved defensive rearrangement of cellular phenotype aimed at neuroprotection, (2) pathological remodeling, when astrocytes acquire new features driving pathology, and (3) astrodegeneration, a type of astroglial atrophy characterized by a loss of homeostatic functions [25].

In particular, astrocyte dysfunction emerges early in AD, and may contribute to its severity and progression [26]. Indeed, prominent astroglia degeneration contributes to neural deficits and cognitive decline [27] through inflammatory response activation and $A\beta$ plaque evolution [28,29].

Initial glia dysfunction, characterized by activated astrocytes expressing elevated levels of GFAP, appears in the very early stages of AD [30]. Interestingly, under these conditions, both genetic deletion and pharmacological inhibition of $K_V3.4$ channel subunits, by possibly counteracting cytoplasmic K^+ loss, are effective in reducing astrocytes' activation [30]. Interestingly, low cytoplasmic K^+ concentrations determine the activation of inflammasome [31,32], mainly involved in AD progression [33,34].

Furthermore, $K_V3.4$ channels mediating fast inactivating K^+ currents (I_A)—mainly contributing to the action potential repolarization—are dysfunctional in AD [30,35–37]. Moreover, cell death caused by the loss of cytoplasmic K^+ concentrations due to the enhanced function of $K_V3.4$ channel upon $A\beta_{1-42}$ exposure has been detected at the neuronal level [37]. Accordingly, a significant correlation has been ascertained between altered intracellular K^+ concentrations and apoptotic processes [38]. In fact, in hippocampal neurons, $K_V3.4$ channel blockade prevents the apoptotic cascade triggered by $A\beta_{1-42}$ [37]. Therefore, $K_V3.4$ channel could be considered a new pharmacological target against AD progression.

In this respect, toxins from marine organisms with a high selectivity towards ion channels [37,39,40] may provide molecular tools to treat ion channel-related diseases [41].

Therefore, in the present study, we have investigated the effect of the *Anemonia sulcata* toxin blood depressing substance-I (BDS-I) blocking $K_V3.4$ channel subunits on $[Ca^{2+}]_i$ transients, ER Ca^{2+} signaling, reactive oxygen species (ROS) production, and cell survival in cortical astrocytes exposed to $A\beta_{1-42}$ oligomers.

2. Results

2.1. Exposure to $A\beta_{1-42}$ Oligomers Upregulated $K_V3.4$ Protein Expression and Activity in Activated Rat Primary Cortical Astrocytes

To examine cytoskeleton rearrangement after exposure to $A\beta_{1-42}$ oligomers, F-actin cytoskeleton was stained in primary cortical astrocytes with the actin-binding dye phalloidin. The filament network was brightly stained in control astrocytes (Figure 1A). However, actin bundle disassembly and body extroflexions revealed pronounced astrogliosis in

astrocytes treated with 5 μM $\text{A}\beta_{1-42}$ oligomers for 48 h (Figure 1A). Confocal double immunofluorescence experiments revealed that the $\text{K}_V3.4$ immunoreactivity was mainly confined along the plasma membrane of control GFAP-positive cortical astrocytes (Figure 1B). Moreover, primary cortical astrocytes exposed to 5 μM $\text{A}\beta_{1-42}$ oligomers for 48 h showed a more pronounced immunoreactivity for both GFAP and $\text{K}_V3.4$ as compared to controls (Figure 1B). Interestingly, the two immunosignals intensely overlapped within the filament bundles (Figure 1B). Furthermore, Western blotting analysis revealed that after 48 h exposure to $\text{A}\beta_{1-42}$ oligomers, $\text{K}_V3.4$ protein expression significantly increased in primary cortical astrocytes as compared to controls (Figure 1C). Accordingly, patch-clamp recordings in whole-cell configuration showed a significant upregulation of the fast-inactivating currents (I_A) in primary cortical astrocytes exposed for 48 h to $\text{A}\beta_{1-42}$ oligomers compared with control astrocytes (Figure 2A). In contrast, 5 μM of the scramble $\text{A}\beta$ peptide ($\text{A}\beta_{42-1}$) did not induce any significant modification of I_A (Figure 2A). Moreover, the contribution of $\text{K}_V3.4$ to I_A upregulation in primary cortical astrocytes exposed to $\text{A}\beta_{1-42}$ oligomers was further tested by blocking this channel with the selective blocker BDS-I. Treatment with BDS-I (50 nM) reduced I_A (Figure 2A) in primary cortical astrocytes exposed to $\text{A}\beta_{1-42}$ oligomers (Figure 2A). Interestingly, electrophysiological patch-clamp recordings in primary cortical astrocytes exposed to $\text{A}\beta_{1-42}$ oligomers (5 μM , 48 h) revealed that firing frequency was lower than in controls (Figure 2B), whereas resting membrane potential was more negative than in controls (Figure 2C). Moreover, BDS-I treatment counteracted either the spike frequency decrease or the membrane hyperpolarization in primary cortical astrocytes exposed to $\text{A}\beta_{1-42}$ oligomers (Figure 2B,C, respectively).

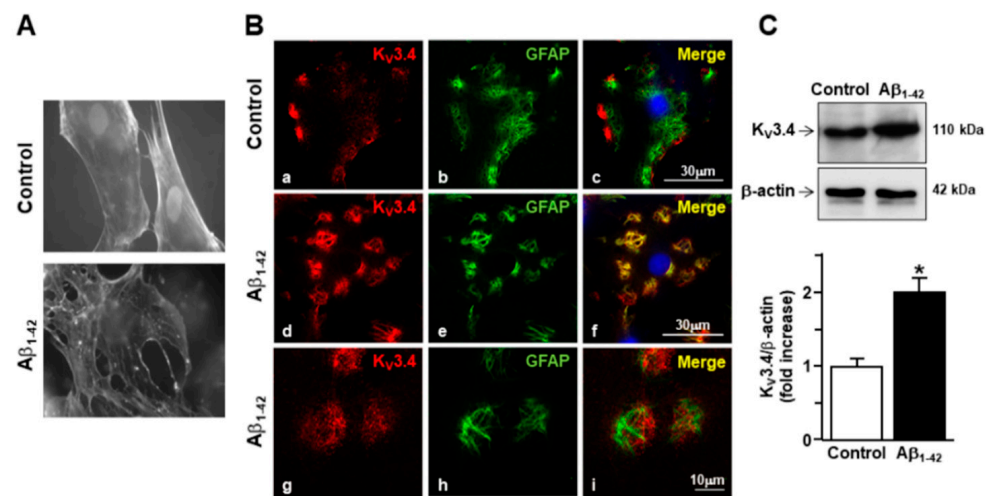


Figure 1. Effect of $\text{A}\beta_{1-42}$ oligomers on the upregulation of $\text{K}_V3.4$ protein expression in rat primary astrocytes. (A) Phalloidin-stained images of rat primary astrocytes under control conditions and 48 h after 5 μM $\text{A}\beta_{1-42}$ exposure. Nuclei were marked by Hoechst 33258. (B) Confocal double immunofluorescence images of rat primary astrocytes displaying both $\text{K}_V3.4$ (red) and glial fibrillary acid protein (GFAP) (green) immunoreactivities under control conditions (a–c) or 48 h after 5 μM $\text{A}\beta_{1-42}$ exposure (d–i). Higher magnification of the frame depicted in g–i displaying intense immuno-positive fiber bundles double-labeled for both $\text{K}_V3.4$ and GFAP in AD astrocytes. Scale bars: a–f: 30 μm ; g–i: 10 μm . (C) Western blotting and densitometric analysis of $\text{K}_V3.4$ protein levels under control conditions or 48 h after 5 μM $\text{A}\beta_{1-42}$ exposure. Data were normalized on the basis of β -actin and expressed as fold increase compared to control's expression of three different preparations. * $p < 0.05$ vs. control.

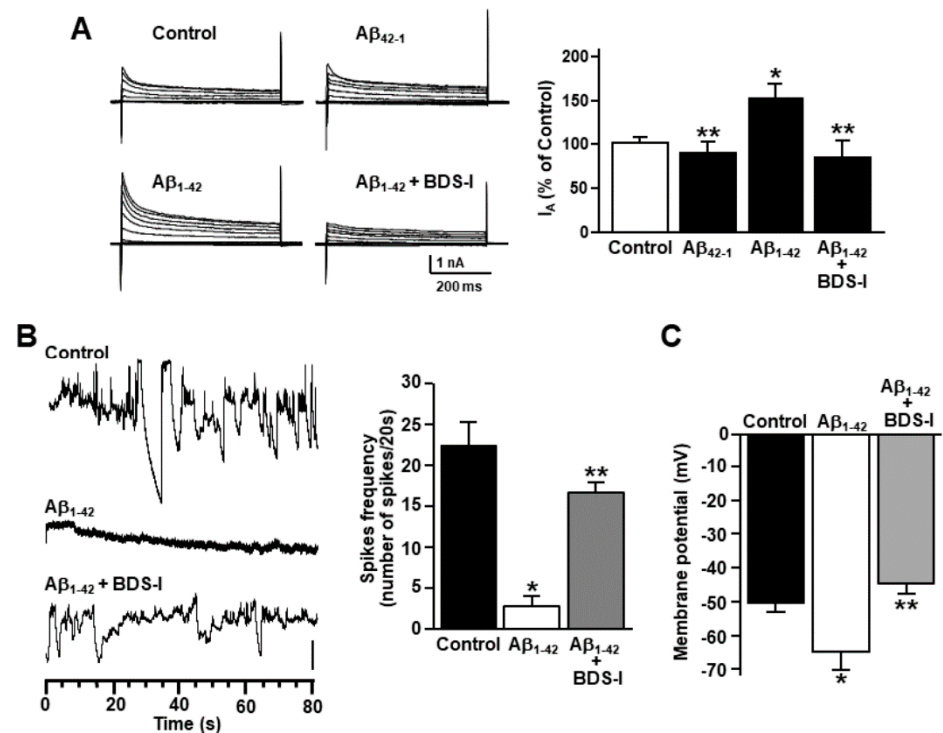


Figure 2. Effect of $A\beta_{1-42}$ oligomers on the upregulation of $K_V3.4$ channel activity in rat primary astrocytes. (A) Representative traces and quantification of $K_V3.4$ -mediated fast inactivating K^+ currents (I_A) recorded from rat primary astrocytes under control conditions, 48 h after 5 μ M $A\beta_{1-42}$ exposure in the absence and in the presence of 50 nM blood depressing substance-I (BDS-I), or 48 h after 5 μ M $A\beta_{42-1}$ exposure. The peak values of I_A , measured at the beginning of the +40mV depolarizing pulse, are expressed as percentage mean \pm standard error of the mean (SEM) of three independent experiments performed on three different preparations ($n = 12$ cells in each cell culture and for each group). * $p < 0.05$ vs. controls; ** $p < 0.05$ vs. $A\beta_{1-42}$. (B) Representative current traces recorded in the gap-free mode under control conditions or 48 h after 5 μ M $A\beta_{1-42}$ exposure in the absence and in the presence of 50 nM BDS-I in rat primary astrocytes. Vertical scale bar below the trace represents 1 pA. (C) Quantification of the effects of $A\beta_{1-42}$ oligomers on membrane potential under control conditions or 48 h after 5 μ M $A\beta_{1-42}$ exposure in the absence and in the presence of 50 nM BDS-I. The values are expressed as mV and represent the mean \pm SEM of three independent experiments performed on three different preparations (for both B and C: $n = 12$ cells for each group). * $p < 0.05$ vs. controls; ** $p < 0.05$ vs. $A\beta_{1-42}$.

2.2. Effects of BDS-I on $[Ca^{2+}]_i$ Transients and ER Ca^{2+} Signaling in Rat Primary Astrocytes Exposed to $A\beta_{1-42}$ Oligomers

Rat primary cortical astrocytes displayed spontaneous $[Ca^{2+}]_i$ transients in the period of control recordings characterized by two main oscillatory patterns with different degrees of irregularity (Figure 3(Aa,b,b')). After 48 h exposure to $A\beta_{1-42}$ oligomers, the frequency of astrocytic $[Ca^{2+}]_i$ transients was significantly reduced (Figure 3(Ba,b,b',D)). In accordance with the electrophysiological experiments aimed to detect spike frequency and membrane potential, BDS-I counteracted the effect of the prolonged exposure to $A\beta_{1-42}$ oligomers on $[Ca^{2+}]_i$ transients, thus quite restoring the resting frequency in a dose-dependent way (Figure 3(Ca,b,b',D)).

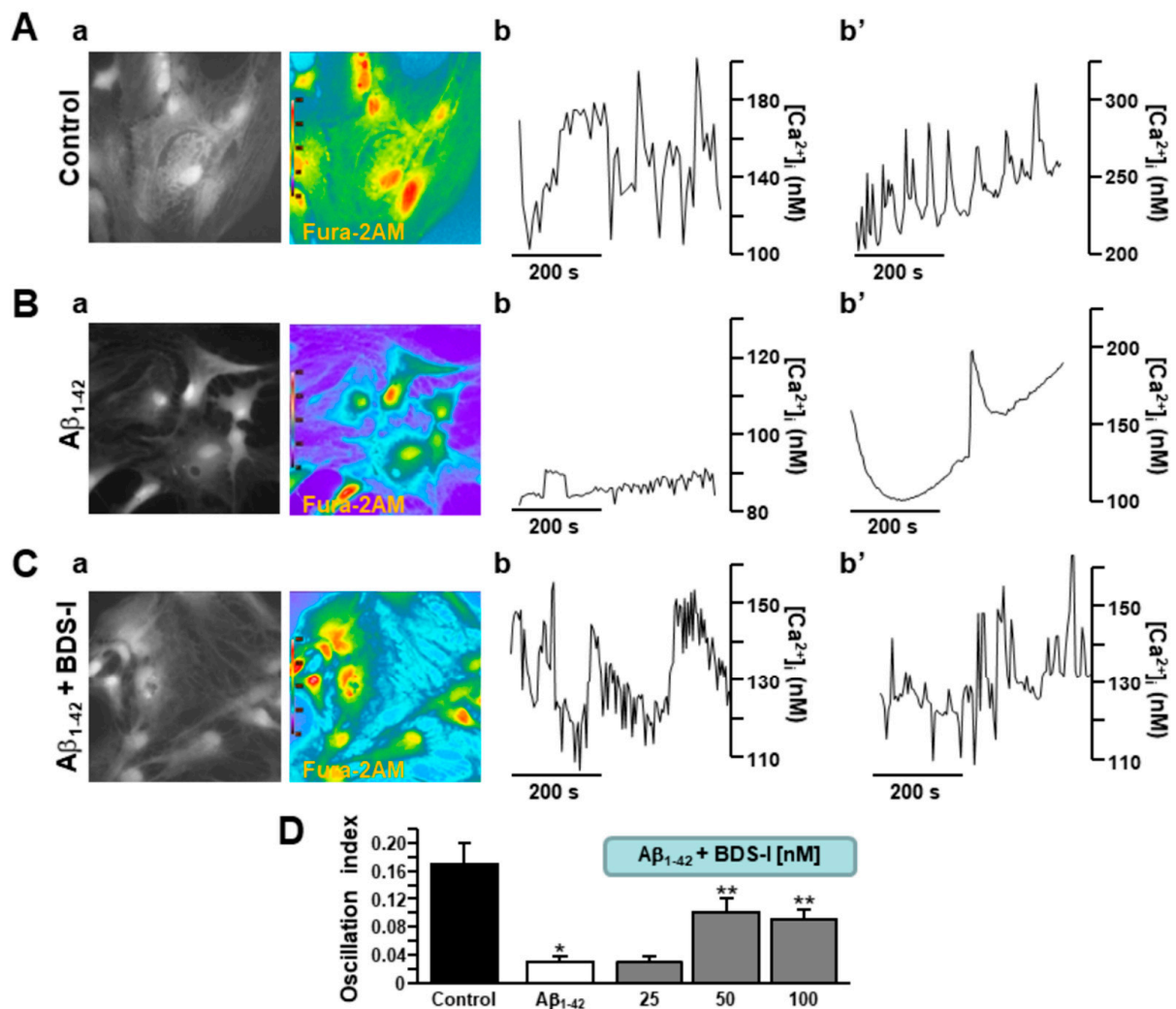


Figure 3. Effects of BDS-I on Aβ₁₋₄₂-dependent modulation of [Ca²⁺]_i transients in rat primary astrocytes. (A) Representative fluorescent images (a) and traces (b,b') of rat primary cortical astrocytes in control conditions displaying two different types of [Ca²⁺]_i transients. Under control conditions, *n* = 30 cells have been recorded in three different experimental sessions. (B) Representative fluorescent images (a) and traces (b,b') of rat primary cortical astrocytes exposed to Aβ₁₋₄₂ oligomers (5 μM, 48 h) displaying two types of reduced [Ca²⁺]_i transients. Under these conditions, *n* = 33 cells have been recorded in three different experimental sessions. (C) Representative fluorescent images (a) and traces (b,b') of rat primary cortical astrocytes exposed simultaneously to Aβ₁₋₄₂ oligomers (5 μM, 48 h) and BDS-I (50 nM) displaying restored [Ca²⁺]_i transients. Under these conditions, *n* = 30 cells have been recorded in three different experimental sessions. (D) Quantification of the oscillatory index in A, B, and C. The experiments with BDS-I have been performed in the nanomolar range of concentrations. Data are reported as mean ± SEM. * *p* < 0.05 vs. control; ** *p* < 0.05 vs. all.

In order to assess the involvement of the major intracellular Ca²⁺-storing organelle in the modulation of [Ca²⁺]_i transients by Aβ₁₋₄₂ oligomers, Ca²⁺ depletion from the ER was induced in cortical astrocytes by ATP and thapsigargin in a nominal Ca²⁺-free solution. Interestingly, after 48 h exposure to Aβ₁₋₄₂ oligomers, ER Ca²⁺ content was higher in AD astrocytes than in controls (Figure 4A,B). Moreover, when astrocytes were incubated with BDS-I together with Aβ₁₋₄₂ oligomers, ER Ca²⁺ content was restored to control level (Figure 4A,B), thus suggesting a putative, and possibly compensatory, involvement of the increased K_v3.4-mediated outward K⁺ currents in the ER Ca²⁺ overload.

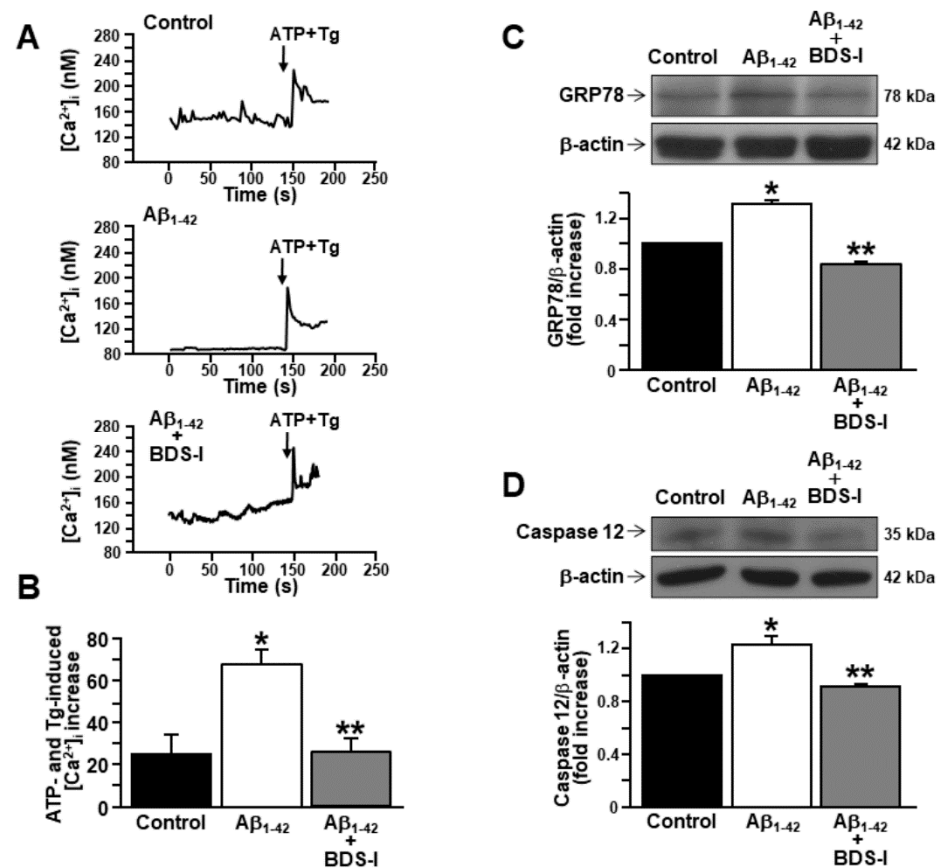


Figure 4. Effects of BDS-I on endoplasmic reticulum (ER) Ca^{2+} level and ER stress markers in rat primary astrocytes exposed to $A\beta_{1-42}$ oligomers. (A) Representative traces of the effect of ATP (100 μ M) + thapsigargin (Tg, 1 μ M) in a nominal Ca^{2+} -free solution on $[Ca^{2+}]_i$ in astrocytes under control conditions (top trace $n = 40$), exposed to $A\beta_{1-42}$ oligomers (5 μ M, 48 h) (middle trace, $n = 48$) or exposed to $A\beta_{1-42}$ oligomers (5 μ M, 48 h) plus BDS-I (50 nM) (bottom trace, $n = 50$). (B) Quantification of A reported as mean \pm SEM. * $p < 0.05$ vs control; ** $p < 0.05$ vs. $A\beta_{1-42}$. (C) Representative Western blotting and densitometric quantification of GRP78/BiP protein expression levels under control conditions or 48 h after 5 μ M $A\beta_{1-42}$ oligomers exposure in the absence and in presence of 50 nM BDS-I. The values were normalized on the basis of β -actin and expressed as fold increase compared to controls of three independent experimental sessions. * $p < 0.05$ vs controls; ** $p < 0.05$ vs. $A\beta_{1-42}$. (D) Representative Western blotting and densitometric quantification of active caspase 12 under control conditions or 48 h after 5 μ M $A\beta_{1-42}$ oligomers exposure in the absence and in presence of 50 nM BDS-I. The values were normalized on the basis of β -actin and expressed as fold increase compared to controls of three independent experimental sessions. * $p < 0.05$ vs. control; ** $p < 0.05$ vs. $A\beta_{1-42}$.

2.3. Effects of BDS-I on ER Stress Markers in Rat Primary Astrocytes Exposed to $A\beta_{1-42}$ Oligomers

Current evidence suggests that Ca^{2+} dysregulation and ER stress still represent two relevant features of $A\beta$ accumulation [24,42,43]. Therefore, the expression of the ER chaperone GRP78/BiP has been studied in astrocytes exposed to $A\beta_{1-42}$ oligomers (5 μ M, 48 h), considering this chaperone as one of the main markers of early AD stage [43]. After 48 h exposure to $A\beta_{1-42}$ oligomers, GRP78/BiP protein expression peaked in AD astrocytes compared with controls (Figure 4C). Importantly, BDS-I prevented GRP78/BiP overexpression when incubated with $A\beta_{1-42}$ oligomers (Figure 4C). Moreover, the expression of active caspase 12 was also upregulated in astrocytes by a long exposure to $A\beta_{1-42}$ oligomers (5 μ M, 48 h) (Figure 4D), while it was prevented in astrocytes simultaneously exposed to BDS-I and $A\beta_{1-42}$ oligomers (Figure 4D).

2.4. Effects of BDS-I on ROS Production, Mitochondrial Activity, and Lactate Dehydrogenase (LDH) Release in Rat Primary Astrocytes Exposed to $A\beta_{1-42}$ Oligomers

Considering that ER stress and dysregulated calcium homeostasis may lead to reactive oxygen species (ROS) formation [42], they were detected in rat primary astrocytes using the specific fluorescent dye 2',7'-dichlorodihydrofluorescein diacetate (DCFH-DA). Furthermore, dysfunction in lactate dehydrogenase (LDH) release and mitochondrial activity were detected as markers of cell suffering in AD astrocytes. ROS production was significantly increased after exposure to $A\beta_{1-42}$ oligomers (5 μ M, 48 h) compared with control cells (Figure 5A), while BDS-I prevented this event in AD astrocytes (Figure 5A). Consistently, BDS-I counteracted the significant reduction in mitochondrial activity and the increased level of LDH release induced by $A\beta_{1-42}$ oligomers in astrocytes (Figure 5B,C, respectively).

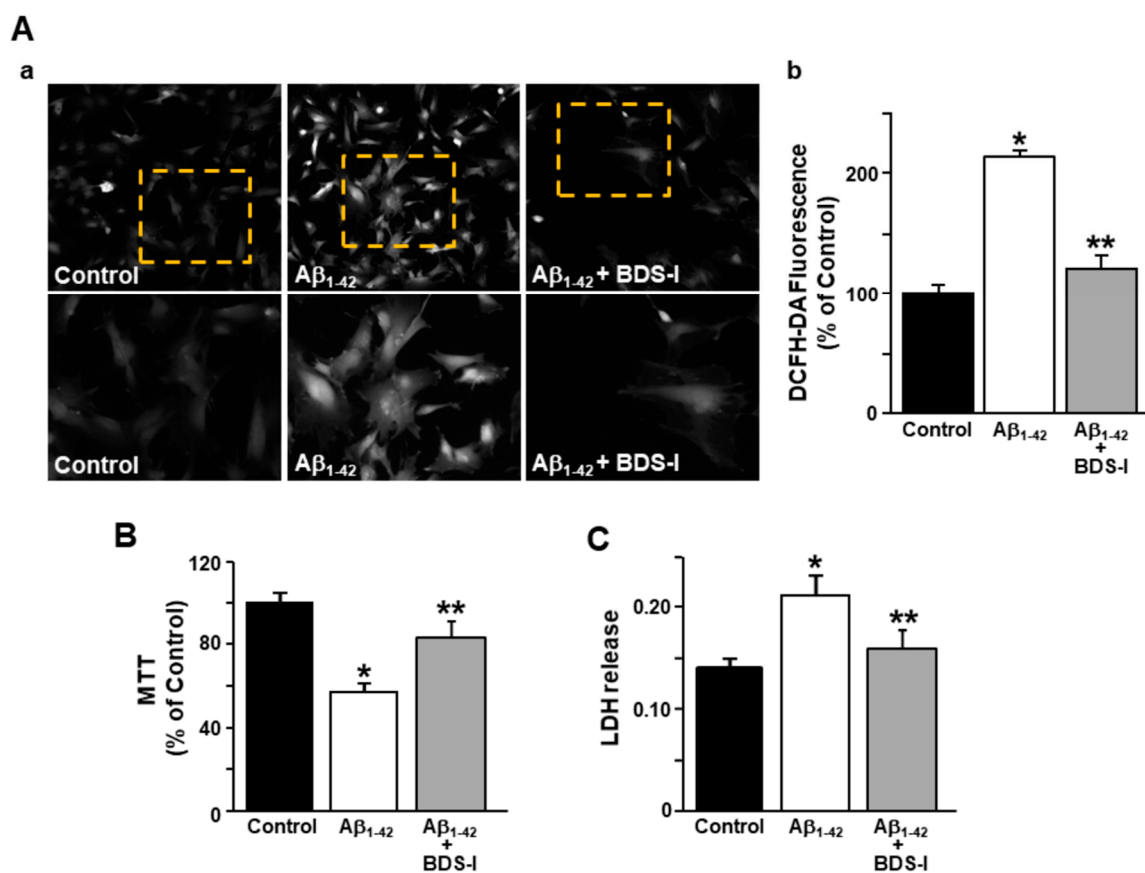


Figure 5. Effects of BDS-I on ROS production, mitochondrial activity, and lactate dehydrogenase (LDH) release in rat primary astrocytes exposed to $A\beta_{1-42}$ oligomers. (A) Representative images (a) and quantification (b) of the fluorescence intensity of 2',7'-dichlorodihydrofluorescein diacetate (DCFH-DA) under control conditions or 48 h after 5 μ M $A\beta_{1-42}$ exposure in the absence and in the presence of 50 nM BDS-I. The values are expressed as percentage mean \pm SEM of three independent experimental sessions. * $p < 0.05$ vs. controls; ** $p < 0.05$ vs. $A\beta_{1-42}$. (B) Quantification of mitochondrial dehydrogenase activity under control conditions or 48 h after 5 μ M $A\beta_{1-42}$ exposure in the absence and in the presence of 50 nM BDS-I. The values are expressed as percentage mean \pm SEM of three independent experimental sessions. * $p < 0.05$ vs. controls; ** $p < 0.05$ vs. $A\beta_{1-42}$. (C) Quantification of LDH release under control conditions or 48 h after 5 μ M $A\beta_{1-42}$ exposure in the absence and in the presence of 50 nM BDS-I. The values are expressed as mean \pm SEM of three independent experimental sessions. * $p < 0.05$ vs. control; ** $p < 0.05$ vs. $A\beta_{1-42}$.

3. Discussion

The present study shows that the *Anemonia sulcata* toxin BDS-I restored spontaneous $[Ca^{2+}]_i$ transients in rat primary astrocytes exposed to $A\beta_{1-42}$ oligomers. This may occur via the inhibition of the hyperfunctional $K_V3.4$ potassium channel, whose expression and activity resulted to be significantly upregulated in $A\beta_{1-42}$ -treated astrocytes. Accordingly,

the expression and function of $K_V3.4$ channel subunits have been previously found to be upregulated in reactive astrocytes in AD Tg2576 mouse brains [30]. The chosen time-point of BDS-I incubation comes from the previous study [30] showing that, nevertheless the upregulation of both $K_V3.4$ potassium channel expression and activity starts before, the GFAP-monitored astrogliosis occurs only at 48 h exposure to $A\beta_{1-42}$ oligomers [30].

In line with our results, both astrocytes associated with senile plaques in APP/PS1 mice [44] and astrocytes from APP_{Swe} mice in an early stage of the disease display atypical Ca^{2+} waves [45].

Moreover, the mechanisms of spontaneous astrocytic $[Ca^{2+}]_i$ transients, mainly involved in important brain functions, are still unclear. In this study, we have identified: (i) a novel mechanism controlling the electrical phenomenon represented by $K_V3.4$ channel subunits and (ii) a new putative molecule with a therapeutic profile.

Furthermore, $K_V3.4$ -mediated I_A currents are dysfunctional in AD not only in neurons but also in glial cells [30,35–37]. In this respect, and in consideration that $K_V3.4$ overexpression intervenes in the neuro-inflammation underlying AD development [30], BDS-I may assume a putative neuroprotective profile. Therefore, controlling the function of $K_V3.4$ channels in AD brain with BDS-I might represent a novel therapeutic approach for slowing down the progression of the disease.

At higher concentrations than that used in the present manuscript, BDS-I is also an efficient modulator of $Na_v1.7$ channel [46]. In fact, BDS-I slows down the inactivation Na^+ channels, but slightly more than the specific toxins AsI, AsII, and AxI from *A. sulcata* and *A. xanthogrammica* [47,48]. Of note, BDS-I has only a small effect on tetrodotoxin (TTX)-sensitive Na^+ channels [49] and no action on voltage-sensitive Na^+ channels in cardiac cells or in skeletal muscle myotubes [39]. Therefore, putative downstream effects associated to its action on Na^+ channels can be hypothesized, although restricted to the site of $Na_v1.7$ localization.

The treatment of cultured astrocytes with exogenous $A\beta$ oligomers induces a pathological remodeling of Ca^{2+} signaling [50] by affecting both neurotransmission machinery and ER Ca^{2+} handling [51]. In particular, under these conditions, changes in inositol 1,4,5-triphosphate receptor (IP_3R) expression with consequent defects in store-operated calcium entry (SOCE) were recorded in astrocytes and in organotypic slices [24]. Of note, astrocytes isolated from 3xTg-AD mice displayed increased SOCE [52] and altered $[Ca^{2+}]_i$ oscillations [53]. Therefore, previous evidence showed the importance of astrocytic Ca^{2+} signaling in AD progression with particular respect to the intracellular component of Ca^{2+} machinery. In line with the burgeoning literature on this issue, the present data show that BDS-I reduced ER Ca^{2+} overload in astrocytes induced by $A\beta_{1-42}$ oligomers with the consequent prevention of the expression of ER stress markers, including active caspase 12 and GRP78/BiP. Indeed, calcium dysregulation, ER stress, and overexpression of unfolded protein response (UPR) elements like GRP78/BiP have been identified as common pathways in neurodegenerative diseases, including AD [24,54,55]. In particular, GRP78/BiP protein expression levels change differently according to the stage of AD: in chronic AD patients, GRP78/BiP expression is very low, while in the early AD stages, GRP78/BiP has been found to be overexpressed [43]. This highlights the putative role of the Ca^{2+} -dependent ER chaperone as an early marker of the disease [43].

Of note, Ca^{2+} homeostasis and ER Ca^{2+} signaling in glia are under the control of other ionic players, including K^+ channels as with Ca^{2+} signaling in a classical model of excitable cells [56]. Accordingly, deregulation of potassium homeostasis may underlie gliosis in AD. Mechanistically, the intermediate-conductance Ca^{2+} -activated K^+ channel $K_{Ca3.1}$ may induce astrogliosis and microglia activation in the disease [57]. Furthermore, $K_{Ca3.1}$, through the regulation of the membrane potential hyperpolarization, induces SOCE potentiation, ER Ca^{2+} overload, and the consequent ER stress in AD astrocytes [58]. Interestingly, gene deletion or pharmacological blockade of astrocytic $K_{Ca3.1}$ reduce ER stress and prevent downstream neuronal loss in APP/PS1 mice [58], thus highlighting the importance of the astrocytic component in neuronal fate during AD progression.

Moreover, in the present study, the new role of astrocytic $K_V3.4$ channel in the modulation of ER Ca^{2+} signaling has been highlighted in an in vitro model of AD.

In this respect, the mechanistic inquiry into AD pathogenesis and progression have recently switched from the neuron-centric doctrine to an astrocyte-centered theory [59]. Besides the evidence on the role of astrocytic K^+ dysregulation during AD, with the present study, we could only partially answer to this enormous issue. In fact, many efforts should be made in the future to address this important question.

In conclusion, by investigating the relationship between $K_V3.4$ channel and calcium signaling in astrocytes exposed to $A\beta_{1-42}$ oligomers, the present study showed that: (i) dysregulation of $K_V3.4$ channel induced an altered Ca^{2+} transient activity and (ii) the *Anemonia sulcata* toxin BDS-I prevented ER stress by reducing $K_V3.4$ potassium channel hyperfunction and restoring spontaneous $[Ca^{2+}]_i$ transients, thus revealing a putative neuroprotective role for this marine toxin.

4. Materials and Methods

4.1. Drugs and Chemicals

$A\beta$ peptides were synthesized by INBIO (Naples, Italy). Rabbit polyclonal antibody against $K_V3.4$ was from Alomone Labs (Jerusalem, Israel). Rabbit polyclonal antibody against caspase 12 was from Santa Cruz Biotechnology Inc. (Dallas, TX, USA). Rabbit polyclonal antibody against GRP78/BiP and rabbit monoclonal antibody against $A\beta$ were from Cell Signaling Technology, Inc. (Danvers, MA, USA). Mouse monoclonal anti- β -actin, and rabbit polyclonal anti-GFAP antibodies, phalloidin-Atto Rho6G, Hoechst 33258, the reversed sequence $A\beta_{42-1}$, trypsin, DNase, dimethyl sulfoxide (DMSO), 1,1,1,3,3,3-hexafluoro-2-propanol (HFIP), and (3[4,5-dimethylthiazol-2-yl]-2,5-diphenyltetrazolium bromide) (MTT) were from Sigma-Aldrich (Milan, Italy). Mouse monoclonal antibody against $K_V3.4$ was from Anova (Walnut, CA, USA). Fura-2AM was from Calbiochem (Darmstadt, Germany). Enhanced chemiluminescent (ECL) reagents and nitrocellulose membranes were from GE Healthcare (Milan, Italy). Dulbecco's modified Eagle's medium (DMEM), fetal bovine serum, penicillin, streptomycin, and L-glutamine were from Gibco (Milan, Italy). Radioimmunoprecipitation assay (RIPA) buffer and protease inhibitor cocktail II were from Roche Diagnostic (Monza, Italy). Nitrocellulose membranes were from GE Healthcare.

4.2. Rat Primary Astrocytes

Primary cultures of rat astrocytes were obtained as previously described [60–62]. This protocol yields 98% of GFAP-positive cells. In brief, dissected cortices from 1- to 2-day-old rat pups were first dissociated enzymatically in a solution containing 0.125% trypsin and 1.5 mg/mL DNase and then, mechanically, in DMEM supplemented with 10% fetal bovine serum, 100 U/mL penicillin, 100 μ g/mL streptomycin, and 2 mM L-glutamine. Cell pellets were plated on poly-L-lysine-coated plates. The medium was changed 24 h after plating and twice a week thereafter. For the mechanical dissociation, they were shaken vigorously to remove non-adherent cells and sub-cultured firstly at 1:3 dilution and then, once they reached confluency, at 1:4 dilution.

4.3. Solubilization of $A\beta_{1-42}$ Peptide and Cellular Treatment

After synthesis, high-performance liquid chromatography and mass spectrometry showed a 95% purity for the yielded $A\beta$ peptides. Lyophilized peptides were resuspended in HFIP at 1 mM, as previously described [63]. The clear solution was dried until complete elimination of the solvent and recovery of the dried powder. Immediately prior to use, the HFIP-treated aliquots were carefully and completely resuspended to a concentration of 5 mM in anhydrous dimethyl sulfoxide (Me_2SO). $A\beta_{1-42}$ and $A\beta_{42-1}$ oligomers were prepared by diluting the peptides at 5 mM concentration to a 100 μ M solution in ice-cold cell culture medium (phenol red-free Ham's F-12, 4 °C for 24 h). Then, the solution was centrifuged at 14,000 rpm at 4 °C for 10 min and the supernatant containing $A\beta_{1-42}$ oligomers

was stored at $-20\text{ }^{\circ}\text{C}$ [63,64]. $\text{A}\beta_{1-42}$ preparation was tested with monoclonal anti- $\text{A}\beta$ antibody, which recognizes an epitope within residues 17–42 of human $\text{A}\beta$ (see Drugs and Chemicals Section). In particular, Western blotting showed a specific band at $\sim 8\text{ kDa}$, corresponding to $\text{A}\beta_{1-42}$ dimers, and a smear ranging from ~ 8 to $\sim 15\text{ kDa}$, comprising lower molecular weight intermediates (trimers), at the highest concentration of $\text{A}\beta_{1-42}$ preparation [63].

4.4. Western Blotting

Astrocytes were washed in phosphate-buffered saline (PBS) and collected by gentle scraping in ice-cold RIPA buffer containing, in mM: 50 Tris pH 7.4, 100 NaCl, 1 Ethylene glycol tetraacetic acid (EGTA), 1 phenylmethylsulfonyl fluoride (PMSF), 1 sodium orthovanadate, 1 NaF, 0.5% NP-40, and 0.2% Sodium dodecyl sulfate (SDS) supplemented with protease inhibitor cocktail II [65]. Then, protein samples were separated on 10% SDS-polyacrylamide gel and transferred onto nitrocellulose membranes. Membranes were incubated with rabbit polyclonal anti- $\text{K}_{\text{v}}3.4$ (1:1000), rabbit polyclonal anti-caspase 12 (1:1000), rabbit polyclonal anti-GRP78/BiP (1:1000), and mouse monoclonal anti- β -actin (1:1000) antibodies. Immunoreactive bands were detected by chemiluminescence (GE Healthcare, Milan, Italy), and the software ImageJ (NIH, Bethesda, MD, USA) was used for densitometric analysis.

4.5. Immunohistochemistry

Immunostaining and confocal immunofluorescence procedures in cells were performed as previously described [56,57]. Cell cultures were fixed in 4% paraformaldehyde in PBS for 30 min and incubated in primary antisera, mouse monoclonal anti- $\text{K}_{\text{v}}3.4$ (1:500), and rabbit polyclonal anti-GFAP (1:1000). Subsequently, they were incubated in a mixture of fluorescent-labeled secondary antibodies. Control experiments were performed as previously described [66,67]. Images were observed with a Zeiss LSM510 META/laser scanning confocal microscope (Göttingen, Germany). Single images were taken with an optical thickness of $0.7\text{ }\mu\text{m}$ and a resolution of 1024×1024 . All images were obtained with a $40\times$ objective with identical laser power settings.

4.6. Assessment of Nuclear and Cytoskeletal Morphology

Cytoskeleton morphology was studied by the staining of actin with rhodamine phalloidin at 1:50 dilution from stock solution of $100\text{ }\mu\text{g}/1\text{ mL}$ in PBS for 15 min at $37\text{ }^{\circ}\text{C}$ [68]. Coverslips were mounted on glass slides and observed by fluorescence microscopy on a Nikon Eclipse E400 microscope (Nikon, Torrance, CA, USA). Digital images were taken with a CoolSnap camera (Media Cybernetics Inc., Silver Spring, MD, USA), stored on the hard-disk of a Pentium III computer, and analyzed with the Image-Pro Plus 4.5 software.

4.7. Electrophysiology

K^{+} currents were recorded from primary cortical astrocytes in control conditions, exposed to $\text{A}\beta_{1-42}$ oligomers in the presence and in the absence of BDS-I with the patch-clamp technique in whole-cell configuration using a commercially available amplifier Axopatch 200B and Digidata 1322A interface (Molecular Devices, San Jose, CA, USA), as previously described [30,37]. In the same experimental conditions, current signals were acquired in gap-free modality using a Digidata 1322A interface using the protocol previously described [63]. Data were acquired using the pClamp software (version 9.0, Molecular Devices) and data analysis was performed using Clampfit software (version 9.0, Molecular Devices). Spontaneous action potential (AP) activity was measured in primary cortical astrocytes in control conditions, exposed to $\text{A}\beta_{1-42}$ oligomers in the presence and in the absence of BDS-I using the protocol previously described [63,69,70]. Importantly, sustained high-quality whole-cell recordings could be maintained for >15 min with a stable membrane potential and AP waveform, confirming that the presence of spontaneous APs was not the result of declining cell health. Spontaneous AP amplitude and

frequency were determined using our own computer program written in Java computer language. Briefly, for each primary cortical astrocyte, the software calculated the AP mean \pm standard deviation (SD) during the baseline recording interval. This was used to define a cutoff identifying AP, which was set at mean AP \pm 2SD. Subsequently, the software identified each value higher than this cut-off point as AP. To quantify AP features in primary cortical astrocytes in control conditions, exposed to A β_{1-42} oligomers in the presence and in the absence of BDS-I, the following parameters were determined: the amplitude, defined as the difference between transient AP and mean basal and the frequency, defined as the number of peaks divided by the duration of observation. The pipette solution contained the following (in mM): 140 KCl, 2 MgCl₂, 10 acido 4-2-idrossietil-1-piperazinil-etansolfonico (HEPES), 10 glucose, 10 EGTA, and 1 Mg-ATP adjusted at pH 7.4 with KOH. The extracellular solution contained the following (in mM): 150 NaCl, 5.4 KCl, 3 CaCl₂, 1 MgCl₂, 10 HEPES, adjusted pH 7.4 with NaOH. 50 nM tetrodotoxin (TTX) and 10 μ M nimodipine were added to Ringer's solution to abolish TTX-sensitive Na⁺, and L-type Ca²⁺ current. The blood-depressing substance-I (BDS-I; synthesized by Prof. P. Grieco, Department of Pharmacy, "Federico II" University of Naples, Naples, Italy) at the concentration of 50 nM was used to block K_V3.4 currents [36,37,40].

Spontaneous action potential (AP) activity was measured in primary cortical astrocytes in control conditions, exposed to A β_{1-42} oligomers in the presence and in the absence of BDS-I using the protocol previously described [63,69,70]. Importantly, sustained high-quality whole-cell recordings could be maintained for > 15 min with a stable membrane potential and AP waveform, confirming that the presence of spontaneous APs was not the result of declining cell health. Spontaneous AP amplitude and frequency were determined using our own computer program written in Java computer language. Briefly, for each primary cortical astrocyte, the software calculated the AP mean \pm standard deviation (SD) during the baseline recording interval. This was used to define a cutoff identifying AP, which was set at mean AP \pm 2SD. Subsequently, the software identified each value higher than this cut-off point as AP. To quantify AP features in primary cortical astrocytes in control conditions, exposed to A β_{1-42} oligomers in the presence and in the absence of BDS-I, the following parameters were determined: the amplitude, defined as the difference between transient AP and mean basal and the frequency, defined as the number of peaks divided by the duration of observation. The pipette solution contained the following (in mM): 140 KCl, 2 MgCl₂, 10 acido 4-2-idrossietil-1-piperazinil-etansolfonico (HEPES), 10 glucose, 10 EGTA, and 1 Mg-ATP adjusted at pH 7.4 with KOH. The extracellular solution contained the following (in mM): 150 NaCl, 5.4 KCl, 3 CaCl₂, 1 MgCl₂, 10 HEPES, adjusted pH 7.4 with NaOH. 50 nM tetrodotoxin (TTX) and 10 μ M nimodipine were added to Ringer's solution to abolish TTX-sensitive Na⁺, and L-type Ca²⁺ current. The blood-depressing substance-I (BDS-I; synthesized by Prof. P. Grieco, Department of Pharmacy, "Federico II" University of Naples, Naples, Italy) at the concentration of 50 nM was used to block K_V3.4 currents [36,37,40].

4.8. [Ca²⁺]_i Measurement

[Ca²⁺]_i was measured by single-cell computer-assisted video-imaging in astrocytes loaded with 10 μ M Fura-2/AM [24,71,72]. [Ca²⁺]_i transients were identified using a software written in Java computer language, as previously reported [71]. Briefly, for each single astrocyte, the software calculated, during the time of recording, the [Ca²⁺]_i mean \pm SD in order to define a cut-off point. Then, the software identified each value higher than this cut-off point as a single [Ca²⁺]_i transient. For each experiment, [Ca²⁺]_i transients were detected during the recordings and used to calculate the oscillation frequency that corresponds to the number of peaks divided by the duration of the recording (oscillation index).

4.9. Measurement of Reactive Oxygen Species

DCFH-DA, a cell membrane permeable fluorescein analogue, was used to detect ROS species production [36]. The rat primary astrocytes were pre-loaded with DCFH-DA

(10 μ M) for 30 min at 37 °C in PBS at the end of each pharmacological treatment. Cells were then washed with PBS, and the reaction was stopped by adding 2,6-di-tert-butyl-4-methylphenol (0.2% in ethanol) and EDTA (2 mM). The cells were then viewed with a Zeiss AxioScope 2FS plus fluorescence microscope (Gottingen, Germany) using excitation and emission wavelengths of 488 and 525 nm, respectively. Digital images were taken with a CoolSnap camera (Media Cybernetics Inc., Silver Spring, MD, USA), and analyzed with the Image-Pro Plus 4.5 software (Media Cybernetics Inc., Silver Spring, MD, USA). Image acquisition and processing were performed equally for all experimental conditions; for the quantification, background fluorescence was subtracted from the data.

4.10. Determination of Mitochondrial Activity

Mitochondrial dysfunction was evaluated with the MTT test [73,74]. In this test, the MTT dye is metabolized by viable mitochondria to a colored product and can be detected photometrically. Briefly, after the experimental procedures, rat primary astrocytes were washed with normal Krebs and incubated with 1 mL of MTT solution (0.5 mg/mL in PBS), as previously described [73,74]. After 1 h incubation at 37 °C, rat primary astrocytes were dissolved in 1 mL of DMSO, in which the rate of MTT reduction was measured using a spectrophotometer at a wavelength of 540 nm. Data are expressed as percentage of mitochondrial dysfunction versus sham-treated cultures.

4.11. LDH Release Assay

Cytotoxicity was detected using a LDH release assay kit (Jiancheng Bioengineering Institute of Nanjing, Jiangsu, China) according to the manufacturer's protocol. Rat primary astrocytes were cultured in 96-well plates (1×10^4 cells/well), and after treatment, supernatants were transferred to clean 96-well plates. Absorbance was analyzed at 450 nm using a Bio-Rad 680 Microplate Reader (Bio-Rad Laboratorie, Hercules, CA, USA) [75].

4.12. Statistical Analysis

Data are expressed as mean \pm standard error of the mean (SEM). Statistical analysis was performed with unpaired *t*-test or one-way analysis of variance followed by Newman-Keuls test. Statistical significance was accepted at the 95% confidence level ($p < 0.05$).

Author Contributions: Conceptualization, A.S. and A.P.; Methodology, I.P., V.T., A.C., R.C., F.B. and V.d.R. Formal Analysis, P.G., R.C. and F.B.; Data Curation, I.P., V.T. and P.G. Writing—Review and Editing, A.S. and A.P.; Funding Acquisition, A.S. and A.P. All authors have read and agreed to the published version of the manuscript.

Funding: This study was supported by the following grants: Progetto Ateneo Federico II to A.P. and Progetto Speciale di Ateneo CA.04_CDA_n_103 27.03.2019 to A.S.

Acknowledgments: The authors kindly thank Paolo Fiore (Engineering Ingegneria Informatica S.p.A. Italy) for designing the software for the measurement of the oscillation index.

Conflicts of Interest: The authors declare no conflict of interest. The authors declare that the research was conducted in the absence of any commercial or financial relationships that could be construed as a potential conflict of interest.

References

1. Santello, M.; Toni, N.; Volterra, A. Astrocyte function from information processing to cognition and cognitive impairment. *Nat. Neurosci.* **2019**, *22*, 154–166. [[CrossRef](#)] [[PubMed](#)]
2. Annunziato, L.; Boscia, F.; Pignataro, G. Ionic transporter activity in astrocytes, microglia, and oligodendrocytes during brain ischemia. *J. Cereb. Blood Flow Metab.* **2013**, *33*, 969–982. [[CrossRef](#)] [[PubMed](#)]
3. Boscia, F.; Begum, G.; Pignataro, G.; Sirabella, R.; Cuomo, O.; Casamassa, A.; Sun, D.; Annunziato, L. Glial Na⁺-dependent ion transporters in pathophysiological conditions. *Glia* **2016**, *64*, 1677–1697. [[CrossRef](#)] [[PubMed](#)]
4. Maragakis, N.J.; Rothstein, J.D. Mechanisms of Disease: Astrocytes in neurodegenerative disease. *Nat. Clin. Pract. Neurol.* **2006**, *2*, 679–689. [[CrossRef](#)] [[PubMed](#)]
5. Sofroniew, M.V.; Vinters, H.V. Astrocytes: Biology and pathology. *Acta Neuropathol.* **2010**, *119*, 7–35. [[CrossRef](#)] [[PubMed](#)]
6. Verkhratsky, A.; Butt, A. *Glial Physiology and Pathophysiology*; Wiley–Blackwell: Oxford, UK, 2013.

7. Pongs, O. Voltage-gated potassium channels: From hyperexcitability to excitement. *FEBS Lett.* **1999**, *452*, 31–35. [[CrossRef](#)]
8. Beiersdorfer, A.; Scheller, A.; Kirchhoff, F.; Lohr, C. Panglial gap junction between astrocytes and olfactory ensheathing cells mediate transmission of Ca²⁺ transients and neurovascular coupling. *Glia* **2019**, *67*, 1385–1400. [[CrossRef](#)]
9. John, G.R.; Scemes, E.; Suadicani, S.O.; Liu, J.S.; Charles, P.C.; Lee, S.C.; Spray, D.C.; Brosnan, C.F. IL-1beta differentially regulates calcium wave propagation between primary human fetal astrocytes via pathways involving P2 receptors and gap junction channels. *Proc. Natl. Acad. Sci. USA* **1999**, *96*, 11613–11618. [[CrossRef](#)]
10. Dani, J.W.; Chernjavsky, A.; Smith, S.J. Neuronal activity triggers calcium waves in hippocampal astrocyte networks. *Neuron* **1992**, *8*, 429–440. [[CrossRef](#)]
11. Araque, A.; Carmignoto, G.; Haydon, P.G.; Oliet, S.H.R.; Robitaille, R.; Volterra, A. Gliotransmitters Travel in Time and Space. *Neuron* **2014**, *81*, 728–739. [[CrossRef](#)]
12. Verkhratsky, A.; Nedergaard, M. Physiology of Astroglia. *Physiol. Rev.* **2018**, *98*, 239–389. [[CrossRef](#)] [[PubMed](#)]
13. Volterra, A.; Liaudet, N.; Savtchouk, I. Astrocyte Ca²⁺ signaling: An unexpected complexity. *Nat. Rev. Neurosci.* **2014**, *15*, 327–335. [[CrossRef](#)] [[PubMed](#)]
14. Panatier, A.; Robitaille, R. Astrocytic mGluR5 and the tripartite synapse. *Neuroscience* **2016**, *323*, 29–34. [[CrossRef](#)] [[PubMed](#)]
15. Khakh, B.S.; McCarthy, K.D. Astrocyte calcium signaling from observations to functions and the challenges therein. *Cold Spring Harb. Perspect. Biol.* **2015**, *7*, a020404. [[CrossRef](#)] [[PubMed](#)]
16. Rusakov, D.A. Disentangling calcium-driven astrocyte physiology. *Nat. Rev. Neurosci.* **2015**, *16*, 226–233. [[CrossRef](#)] [[PubMed](#)]
17. Shigetomi, E.; Patel, S.; Khakh, B.S. Probing the complexities of astrocyte calcium signaling. *Trends Cell Biol.* **2016**, *26*, 300–312. [[CrossRef](#)]
18. Semyanov, A. Spatiotemporal pattern of calcium activity in astrocytic network. *Cell Calcium* **2019**, *78*, 15–25. [[CrossRef](#)]
19. Hertz, L. Possible role of neuroglia: A potassium-mediated neuronal-neuroglial-neuronal impulse transmission system. *Nature* **1965**, *206*, 1091–1094. [[CrossRef](#)]
20. Orkland, R.K.; Nicolls, G.J.; Kuffler, S.W. Effect of nerve impulses on the membrane potential of glial cells in the central nervous system of amphibia. *J. Neurophysiol.* **1966**, *29*, 788–806. [[CrossRef](#)]
21. David, Y.; Cacheaux, L.P.; Ivens, S.; Lapilover, E.; Heinemann, U.; Kaufer, D.; Friedman, A. Astrocytic dysfunction in epileptogenesis: Consequence of altered potassium and glutamate homeostasis? *J. Neurosci.* **2009**, *29*, 10588–10599. [[CrossRef](#)]
22. Leis, J.A.; Bekar, L.K.; Walz, W. Potassium homeostasis in the ischemic brain. *Glia* **2005**, *50*, 407–416. [[CrossRef](#)] [[PubMed](#)]
23. Pchitskaya, E.; Popugaeva, E.; Bezprozvanny, I. Calcium signaling and molecular mechanisms underlying neurodegenerative diseases. *Cell Calcium* **2018**, *70*, 87–94. [[CrossRef](#)] [[PubMed](#)]
24. Alberdi, E.; Wyssenbach, A.; Alberdi, M.; Sánchez-Gómez, M.V.; Cavaliere, F.; Rodríguez, J.J.; Verkhratsky, A.; Matute, C. Ca²⁺-dependent endoplasmic reticulum stress correlates with astrogliosis in oligomeric amyloid β -treated astrocytes and in a model of Alzheimer's disease. *Aging Cell* **2013**, *12*, 292–302. [[CrossRef](#)] [[PubMed](#)]
25. Verkhratsky, A. Astroglial Calcium Signaling in Aging and Alzheimer's Disease. *Cold Spring Harb. Perspect. Biol.* **2019**, *11*, a035188. [[CrossRef](#)] [[PubMed](#)]
26. Zhao, J.; O'Connor, T.; Vassar, R. The contribution of activated astrocytes to A β production: Implications for Alzheimer's disease pathogenesis. *J. Neuroinflamm.* **2011**, *8*, 150. [[CrossRef](#)]
27. Verkhratsky, A.; Olabarria, M.; Noristani, H.N.; Yeh, C.Y.; Rodriguez, J.J. Astrocytes in Alzheimer's disease. *Neurotherapeutics* **2010**, *7*, 399–412. [[CrossRef](#)]
28. Nagele, R.G.; D'Andrea, M.R.; Lee, H.; Venkataraman, V.; Wang, H.Y. Astrocytes accumulate A beta 42 and give rise to astrocytic amyloid plaques in Alzheimer disease brains. *Brain Res.* **2003**, *971*, 197–209. [[CrossRef](#)]
29. Nagele, R.G.; Wegiel, J.; Venkataraman, V.; Imaki, H.; Wang, K.C.; Wegiel, J. Contribution of glial cells to the development of amyloid plaques in Alzheimer's disease. *Neurobiol. Aging* **2004**, *25*, 663–674. [[CrossRef](#)]
30. Boscia, F.; Pannaccione, A.; Ciccone, R.; Casamassa, A.; Franco, C.; Piccialli, I.; de Rosa, V.; Vinciguerra, A.; Di Renzo, G.; Annunziato, L. The expression and activity of K_v3.4 channel subunits are precociously upregulated in astrocytes exposed to A β oligomers and in astrocytes of Alzheimer's disease Tg2576 mice. *Neurobiol. Aging* **2017**, *54*, 187–198. [[CrossRef](#)]
31. Pétrilli, V.; Papin, S.; Dostert, C.; Mayor, A.; Martinon, F.; Tschopp, J. Activation of the NALP3 inflammasome is triggered by low intracellular potassium concentration. *Cell Death Differ.* **2007**, *14*, 1583–1589. [[CrossRef](#)]
32. Freeman, L.; Guo, H.; David, C.N.; Brickey, W.J.; Jha, S.; Ting, J.P. NLR members NLRC4 and NLRP3 mediate sterile inflammasome activation in microglia and astrocytes. *J. Exp. Med.* **2017**, *214*, 1351–1370. [[CrossRef](#)] [[PubMed](#)]
33. Salminen, A.; Ojala, J.; Suuronen, T.; Kaarniranta, K.; Kauppinen, A. Amyloid-beta oligomers set fire to inflammasomes and induce Alzheimer's pathology. *J. Cell. Mol. Med.* **2008**, *12*, 2255–2262. [[CrossRef](#)]
34. Ebrahimi, T.; Rust, M.; Kaiser, S.N.; Slowik, A.; Beyer, C.; Koczulla, A.R.; Schulz, J.B.; Habib, P.; Bach, J.P. α 1-antitrypsin mitigates NLRP3-inflammasome activation in amyloid β 1–42-stimulated murine astrocytes. *J. Neuroinflamm.* **2018**, *15*, 282. [[CrossRef](#)] [[PubMed](#)]
35. Angulo, E.; Noé, V.; Casadó, V.; Mallol, J.; Gomez-Isla, T.; Lluís, C.; Ferrer, I.; Ciudad, C.J.; Franco, R. Up-regulation of the Kv3.4 potassium channel subunit in early stages of Alzheimer's disease. *J. Neurochem.* **2004**, *91*, 547–557. [[CrossRef](#)] [[PubMed](#)]
36. Pannaccione, A.; Secondo, A.; Scorziello, A.; Cali, G.; Tagliatalata, M.; Annunziato, L. Nuclear factor-kappaB activation by reactive oxygen species mediates voltage-gated K⁺ current enhancement by neurotoxic beta-amyloid peptides in nerve growth factor-differentiated PC-12 cells and hippocampal neurones. *J. Neurochem.* **2005**, *94*, 572–586. [[CrossRef](#)]

37. Pannaccione, A.; Boscia, F.; Scorziello, A.; Adornetto, A.; Castaldo, P.; Sirabella, R.; Tagliatela, M.; Di Renzo, G.F.; Annunziato, L. Up-regulation and increased activity of $K_V3.4$ channels and their accessory subunit MinK-related peptide 2 induced by amyloid peptide are involved in apoptotic neuronal death. *Mol. Pharmacol.* **2007**, *72*, 665–673. [[CrossRef](#)]
38. Yu, S.P. Regulation and critical role of potassium homeostasis in apoptosis. *Prog. Neurobiol.* **2003**, *70*, 363–386. [[CrossRef](#)]
39. Diochot, S.; Schweitz, H.; Béress, L.; Lazdunski, M. Sea anemone peptides with a specific blocking activity against the fast inactivating potassium channel $K_V3.4$. *J. Biol. Chem.* **1998**, *273*, 6744–6749. [[CrossRef](#)]
40. Ciccone, R.; Piccialli, I.; Grieco, P.; Merlino, F.; Annunziato, L.; Pannaccione, A. Synthesis and pharmacological evaluation of a novel peptide based on *Anemonia sulcata* BDS-I Toxin as a new $K_V3.4$ inhibitor exerting a neuroprotective effect against amyloid- β Peptide. *Front. Chem.* **2019**, *7*, 479. [[CrossRef](#)]
41. Finol-Urdaneta, R.K.; Belovanovic, A.; Micic-Vicovac, M.; Kinsella, G.K.; McArthur, J.R.; Al-SabiMarine, A. Toxins Targeting Kv1 Channels: Pharmacological Tools and Therapeutic Scaffolds. *Mar. Drugs* **2020**, *18*, 173. [[CrossRef](#)]
42. Mattson, M.P. Calcium and neurodegeneration. *Aging Cell* **2007**, *6*, 337–350. [[CrossRef](#)] [[PubMed](#)]
43. Lee, J.H.; Won, S.M.; Suh, J.; Son, S.J.; Moon, G.J.; Park, U.J.; Gwag, B.J. Induction of the unfolded protein response and cell death pathway in Alzheimer's disease, but not in aged Tg2576 mice. *Exp. Mol. Med.* **2010**, *42*, 386–394. [[CrossRef](#)] [[PubMed](#)]
44. Kuchibhotla, K.V.; Lattarulo, C.R.; Hyman, B.T.; Bacskai, B.J. Synchronous hyperactivity and intercellular calcium waves in astrocytes in Alzheimer mice. *Science* **2009**, *323*, 1211–1215. [[CrossRef](#)] [[PubMed](#)]
45. Takano, T.; Han, X.; Deane, R.; Zlokovic, B.; Nedergaard, M. Two-photon imaging of astrocytic Ca^{2+} signaling and microvasculature in experimental mice models of Alzheimer's disease. *Ann. N. Y. Acad. Sci.* **2007**, *1097*, 40–50. [[CrossRef](#)]
46. Liu, P.; Jo, S.; Bean, B.P. Modulation of neuronal sodium channels by the sea anemone peptide BDS-I. *J. Neurophysiol.* **2012**, *107*, 3155–3167. [[CrossRef](#)]
47. Frelin, C.; Vigne, P.; Schweitz, H.; Lazdunski, M. The interaction of sea anemone and scorpion neurotoxins with tetrodotoxin-resistant Na^+ channels in rat myoblasts. A comparison with Na^+ channels in other excitable and non-excitable cells. *Mol. Pharmacol.* **1984**, *26*, 70–74.
48. Norton, R.S. Structure and structure-function relationships of sea anemone proteins that interact with the sodium channel. *Toxicon* **1991**, *29*, 1051–1084. [[CrossRef](#)]
49. Vincent, J.P.; Balerna, M.; Barhanin, J.; Fosset, M.; Lazdunski, M. Binding of sea anemone toxin to receptor sites associated with gating system of sodium channel in synaptic nerve endings in vitro. *Proc. Natl. Acad. Sci. USA* **1980**, *77*, 1646–1650. [[CrossRef](#)]
50. Lim, D.; Rodriguez-Arellano, J.J.; Parpura, V.; Zorec, R.; Zeidán-Chuliá, F.; Genazzani, A.A.; Verkhratsky, A. Calcium signalling toolkits in astrocytes and spatio-temporal progression of Alzheimer's disease. *Curr. Alzheimer Res.* **2016**, *13*, 359–369. [[CrossRef](#)]
51. Lim, D.; Iyer, A.; Ronco, V.; Grolla, A.A.; Canonico, P.L.; Aronica, E.; Genazzani, A.A. Amyloid β deregulates astroglial mGluR5-mediated calcium signaling via calcineurin and $Nf-kB$. *Glia* **2013**, *61*, 1134–1145. [[CrossRef](#)]
52. Ronco, V.; Grolla, A.A.; Glasnov, T.N.; Canonico, P.L.; Verkhratsky, A.; Genazzani, A.A.; Dmitry Lim, D. Differential deregulation of astrocytic calcium signaling by amyloid- β , $TNF\alpha$, $IL-1\beta$ and LPS. *Cell Calcium* **2014**, *55*, 219–229. [[CrossRef](#)] [[PubMed](#)]
53. Stenovec, M.; Trkov, S.; Lasic, E.; Terzieva, S.; Kreft, M.; Arellano, J.J.R.; Parpura, V.; Verkhratsky, A. Expression of familial Alzheimer disease presenilin 1 gene attenuates vesicle traffic and reduces peptide secretion in cultured astrocytes devoid of pathologic tissue environment. *Glia* **2016**, *64*, 317–329. [[CrossRef](#)] [[PubMed](#)]
54. Gorbatyuk, M.S.; Gorbatyuk, O.S. The Molecular Chaperone GRP78/BiP as a Therapeutic Target for Neurodegenerative Disorders: A Mini Review. *J. Genet. Syndr. Gene Ther.* **2013**, *4*, 128. [[CrossRef](#)] [[PubMed](#)]
55. Moreno, J.A.; Tiffany-Castiglioni, E. The chaperone Grp78 in protein folding disorders of the nervous system. *Neurochem. Res.* **2015**, *40*, 329–335. [[CrossRef](#)] [[PubMed](#)]
56. Secondo, A.; Tagliatela, M.; Cataldi, M.; Giorgio, G.; Valore, M.; Di Renzo, G.; Annunziato, L. Pharmacological blockade of ERG K^+ channels and Ca^{2+} influx through store-operated channels exerts opposite effects on intracellular Ca^{2+} oscillations in pituitary GH₃ cells. *Mol. Pharmacol.* **2000**, *58*, 1115–1128. [[CrossRef](#)] [[PubMed](#)]
57. Yi, M.; Yu, P.; Lu, Q.; Geller, H.M.; Yu, Z.; Chen, H. $KCa3.1$ constitutes a pharmacological target for astrogliosis associated with Alzheimer's disease. *Mol. Cell.* **2016**, *76*, 21–32. [[CrossRef](#)]
58. Yu, Z.; Dou, F.; Wang, Y.; Hou, L.; Chen, H. Ca^{2+} -dependent endoplasmic reticulum stress correlation with astrogliosis involves upregulation of $KCa3.1$ and inhibition of AKT/mTOR signaling. *J. Neuroinflamm.* **2018**, *15*, 316. [[CrossRef](#)]
59. Verkhratsky, A.; Parpura, V.; Rodriguez-Arellano, J.J.; Zorec, R. Astroglia in Alzheimer's disease. *Adv. Exp. Med. Biol.* **2019**, *1175*, 237–324.
60. Boscia, F.; Gala, R.; Pannaccione, A.; Secondo, A.; Scorziello, A.; Di Renzo, G.; Annunziato, L. NCX1 expression and functional activity increase in microglia invading the infarct core. *Stroke* **2009**, *40*, 3608–3617. [[CrossRef](#)]
61. Boscia, F.; D'Avanzo, C.; Pannaccione, A.; Secondo, A.; Casamassa, A.; Formisano, L.; Guida, N.; Sokolow, S.; Herchuelz, A.; Annunziato, L. Silencing or knocking out the Na^+/Ca^{2+} exchanger-3 (NCX3) impairs oligodendrocyte differentiation. *Cell Death Differ.* **2012**, *19*, 562–572. [[CrossRef](#)]
62. Florio, E.; Keller, S.; Coretti, L.; Affinito, O.; Scala, G.; Errico, F.; Fico, A.; Boscia, F.; Sisalli, M.J.; Reccia, M.G.; et al. Tracking the evolution of epialleles during neural differentiation and brain development: D-Aspartate oxidase as a model gene. *Epigenetics* **2017**, *12*, 41–54. [[CrossRef](#)] [[PubMed](#)]

63. Ciccone, R.; Franco, C.; Piccialli, I.; Boscia, F.; Casamassa, A.; de Rosa, V.; Cepparulo, P.; Cataldi, M.; Annunziato, L.; Pannaccione, A. Amyloid β -Induced Upregulation of Nav1.6 Underlies Neuronal Hyperactivity in Tg2576 Alzheimer's Disease Mouse Model. *Sci. Rep.* **2019**, *9*, 1–18. [[CrossRef](#)] [[PubMed](#)]
64. Stine, W.B.; Dahlgren, K.D.; Krafft, G.A.; LaDu, M.J. In vitro characterization of conditions for amyloid-beta peptide oligomerization and fibrillogenesis. *J. Biol. Chem.* **2003**, *278*, 11612–11622. [[CrossRef](#)] [[PubMed](#)]
65. Esposito, F.; Boscia, F.; Gigantino, V.; Tornincasa, M.; Fusco, A.; Franco, R.; Chieffi, P. The high-mobility group A1-estrogen receptor β nuclear interaction is impaired in human testicular seminomas. *J. Cell Physiol.* **2012**, *227*, 3749–3755. [[CrossRef](#)]
66. Boscia, F.; Ferraguti, F.; Moroni, F.; Annunziato, L.; Pellegrini-Giampietro, D.E. mGlu1 α and CB1 receptors are co-expressed in a subset of interneurons in the CA1 region of organotypic hippocampal slice cultures and adult rat brain. *Neuropharmacology* **2008**, *55*, 428–439. [[CrossRef](#)]
67. Boscia, F.; Esposito, C.L.; Casamassa, A.; de Franciscis, V.; Annunziato, L.; Cerchia, L. The isolectin IB4 binds RET receptor tyrosine kinase in microglia. *J. Neurochem.* **2013**, *126*, 428–436. [[CrossRef](#)]
68. Levee, M.G.; Dabrowska, M.I.; Lelli, J.L.; Hinshaw, D.B. Actin polymerization and depolymerization during apoptosis in HL-60 cells. *Am. J. Physiol.* **1996**, *271*, 1981–1992. [[CrossRef](#)]
69. Bedi, S.S.; Yang, Q.; Crook, R.J.; Du, J.; Wu, Z.; Fishman, H.M.; Grill, R.J.; Carlton, S.M.; Walters, E.T. Chronic spontaneous activity generated in the somata of primary nociceptors is associated with pain-related behavior after spinal cord injury. *J. Neurosci.* **2010**, *30*, 14870–14882. [[CrossRef](#)]
70. Gunhanlar, N.; Shpak, G.; van der Kroeg, M.; Gouty-Colomer, L.A.; Munshi, S.T.; Lendemeijer, B.; Ghazvini, M.; Dupont, C.; Hoogendijk, W.J.G.; Gribnau, J.; et al. A simplified protocol for differentiation of electrophysiologically mature neuronal networks from human induced pluripotent stem cells. *Mol. Psychiatry* **2018**, *23*, 1336–1344. [[CrossRef](#)]
71. Secondo, A.; Pannaccione, A.; Cataldi, M.; Sirabella, R.; Formisano, L.; Di Renzo, G.; Annunziato, L. Nitric oxide induces $[Ca^{2+}]_i$ oscillations in pituitary GH₃ cells: Involvement of IDR and ERG K⁺ currents. *Am. J. Physiol. Cell Physiol.* **2006**, *290*, C233–C243. [[CrossRef](#)]
72. Petrozziello, T.; Secondo, A.; Tedeschi, V.; Esposito, A.; Sisalli, M.; Scorziello, A.; Di Renzo, G.; Annunziato, L. ApoSOD1 lacking dismutase activity neuroprotects motor neurons exposed to beta-methylamino-L-alanine through the Ca²⁺ /Akt/ERK1/2 prosurvival pathway. *Cell Death Differ.* **2017**, *24*, 511–522. [[CrossRef](#)] [[PubMed](#)]
73. Holt, P.S.; Buckley, S.; Deloach, J.R. Detection of the lethal effects of T-2 mycotoxin on cells using a rapid colorimetric viability assay. *Toxicol. Lett.* **1987**, *39*, 301–312. [[CrossRef](#)]
74. Amoroso, S.; Gioielli, A.; Cataldi, M.; Di Renzo, G.F.; Annunziato, L. In the neuronal cell line SH-SY5Y, oxidative stress-induced free radical overproduction causes cell death without any participation of intracellular Ca²⁺ increase. *Biochim. Biophys. Acta* **1999**, *1452*, 151–160. [[CrossRef](#)]
75. Chang, J.; Yang, B.; Zhou, Y.; Yin, C.; Liu, T.; Qian, H.; Xing, G.; Wang, S.; Li, F.; Zhang, Y.; et al. Acute Methylmercury Exposure and the Hypoxia-Inducible Factor-1 α Signaling Pathway under Normoxic Conditions in the Rat Brain and Astrocytes in vitro. *Environ. Health Perspect.* **2019**, *127*, 127006. [[CrossRef](#)] [[PubMed](#)]